Published in final edited form as:

Nat Genet. 2011 June ; 43(6): 579–584. doi:10.1038/ng.813.

Alteration of the serine protease PRSS56 causes angle-closure glaucoma in mice and posterior microphthalamia in humans and mice

K Saidas Nair[1,6], **Mounira Hmani-Aifa**[2,6], **Zain Ali**[1], **Alison L Kearney**[1], **Salma Ben Salem**[2], **Danilo G Macalinao**[1], **Ioan M Cosma**[1], **Walid Bouassida**[3], **Bochra Hakim**[2], **Zeineb Benzina**[3], **Ileana Soto**[1], **Peter Söderkvist**[4], **Gareth R Howell**[1], **Richard S Smith**[1], **Hammadi Ayadi**[2], and **Simon W M John**[1,5]

[1]Howard Hughes Medical Institute, The Jackson Laboratory, Bar Harbor, Maine, USA.

[2]Equipe Procédés de Criblages Moléculaires et Cellulaires, Laboratoire de Microorganismes et Biomolécules, Centre de Biotechnologie de Sfax, Université de Sfax, Sfax Tunisia.

[3]Service d'ophtalmologie, Centre Hospitalo-Universitaire Habib Bourguiba, Sfax, Tunisia.

[4]Division of Cell Biology, Department of Clinical and Experimental Medicine, Faculty of Health Sciences, SE-58185, Linköping, Sweden.

[5]Department of Ophthalmology, Tufts University School of Medicine, Boston, Massachusetts, USA.

[6]*These authors contributed equally to this work*.

Abstract

Angle-closure glaucoma (ACG) is a subset of glaucoma affecting 16 million people[1–3]. Although 4 million people are bilaterally blind from ACG[4,5], the causative molecular mechanisms of ACG remain to be defined. High intraocular pressure induces glaucoma in ACG. High intraocular pressure traditionally was suggested to result from the iris blocking or closing the angle of the eye,

Correspondence should be addressed to S.W.M.J. (simon.john@jax.org) or M.H.-A. (hmanimounira@yahoo.fr)..

AUTHOR CONTRIBUTIONS

K.S.N. conceived and executed experiments and participated in study design, data interpretation and manuscript preparation. Z.A. participated in characterization of the protease and maintenance of the mouse strains, genotyping and phenotyping. A.L.K. participated in fine mapping, sequencing of candidate genes, maintenance of mouse strains and histological assessment. I.M.C. contributed to mutant identification, gene mapping and phenotyping. D.G.M. performed physiological experiments. I.S. participated in cell-biology–based experiments. G.R.H. participated in overall design of gene mapping and histological assessment. R.S.S. contributed to histological assessment and interpretation. S.W.M.J. conceived the study, oversaw all aspects of the study, participated in design, conducting experiments, data interpretation and manuscript preparation.

M.H.-A. contributed to experimental design for human families and conducted experiments and participated in data analysis and manuscript preparation. S.B.S. participated in sequencing of human candidate genes. W.B. is an ophthalmologist and performed clinical evaluation of the patients. Z.B. is also an ophthalmologist and performed clinical evaluation of the patients. B.H. participated in human gene sequencing. P.S. provided advice and help with sequencing of some human candidate genes. H.A. oversaw the human study and participated in data analysis.

URLs. UCSC Human Genome database, http://genome.ucsc.edu, March 2006 release.

Accession codes

The data from this study are deposited in Genbank under the accession code: Mouse *Prss56* cDNA, JF698684. The reference sequences in this study are available from GenBank under the following accession codes: human *PRSS56* cDNA, NM_001195129; human PRSS56 protein, NP_001182058.

thereby limiting aqueous humor drainage. Eyes from individuals with ACG often have a modestly decreased axial length, shallow anterior chamber and relatively large lens, features that predispose to angle closure[6]. Here, we show that genetic alteration of a previously unidentified serine protease alters axial length and causes a mouse phenotype resembling ACG. Mutations affecting this protease also cause a severe decrease of axial length in individuals with posterior microphthalmia. Together, these data suggest that alterations of this serine protease may contribute to a spectrum of human ocular conditions including reduced ocular size and ACG.

The genetic and molecular mechanisms of intraocular pressure (IOP) elevation in ACG are not understood and likely involve a variety of physiological disturbances[7,8]. Mechanistically, IOP elevation is now known to be more complicated than simple blockage of aqueous humor (AqH) drainage by the iris, and reduced ocular dimensions alone are not sufficient to elevate IOP[7]. To identify new genes and mechanisms that impact IOP elevation, we conducted an *N*-ethyl-*N*-nitrosourea (ENU) mutagenesis screen[9] (Online Methods). We identified mutant mice with elevated IOP but otherwise grossly normal eyes (**Fig. 1a**). We named the recessively inherited mutant allele that underlies this phenotype ‘glaucoma relevant mutant 4’ (*Grm4*). The incidence of high IOP in homozygous *Grm4* mutants increased with age (detected in ~50% of mice at 3 months and ~90% of mice at 12 months of age; **Fig. 1b,c**), and the anterior chambers became enlarged in some eyes at around 3 months of age. A histological analysis showed that the angles were not occluded with abnormal tissue (synechia) and had a readily detectable trabecular meshwork and Schlemm's canal (two important drainage structures; **Fig. 1d**). Despite this, compromised AqH drainage (outflow) contributes to the IOP elevation (**Fig. 1e**). After IOP elevation, *Grm4* mutants developed glaucomatous neurodegeneration, which is characterized by retinal ganglion cell death and optic nerve atrophy (**Fig. 1f** and **Supplementary Fig. 1**).

Although mutant eyes appeared grossly normal in size (**Fig. 2a,b**), measurement of enucleated eyes identified a variable reduction of axial length, with values that overlap with controls. On average, the axial length of a randomly selected set of adult mutant eyes was 4.4% shorter than that of wild-type littermate controls at 2 months of age (with a range of 0–10% shorter axial lengths; *t* test $P = 0.015$; **Fig. 2c**). The lens diameter was not different between these groups (*t* test $P = 0.21$; **Fig. 2d**), suggesting that the lens occupies a greater proportion of the ocular volume in mutants. These differences in ocular size occur after birth, and there was no difference in axial length at postnatal day (P) 7, a 3.8% difference at P13 and a 5.1% difference at P20 (**Fig. 2e,f**). Many human eyes with ACG have a reduced axial length and increased lens-to-ocular volume[2,3,6].

Because angle closure is dynamic and is affected by ocular anatomy and unknown physiologic factors, we next evaluated the angle and iris *in vivo*. Gonioscopy allowed viewing of the drainage structures in the angles of all wild-type mice. In contrast, the iris prevented us from viewing these structures in all evaluated mutants (**Fig. 3a**). This is consistent with susceptibility of mutants to angle closure. Optical coherence tomography (OCT) showed that the angle was narrow and the iris was closely apposed to the trabecular meshwork in mutant mice (**Fig. 3b**). This configuration is clearly distinct from that of wild-type mice and matches that in human eyes with ACG. Uveal effusion, characterized by

suprachoroidal fluid accumulation and an expanded choroid[10], is present in many people with ACG[8,11]. Choroidal effusion and expansion may contribute to angle closure and IOP elevation[7,12]. In mutant mice, the choroid is expanded at ages as early as 2 months (**Fig. 3c,d**). To functionally assess the susceptibility of mutant eyes to angle closure, we induced pupil dilation. Pupil dilation exacerbates crowding of the iris in the angle and is known to precipitate angle closure in susceptible eyes[3,13]. Providing further evidence for angle closure in these eyes, pupil dilation induced a large increase in IOP and substantial enlargement of the anterior chamber in some mutant but in no wild-type mice (**Fig. 3e–g**).

To provide molecular insight into mechanisms affecting ocular size as well as mechanisms leading to angle closure and IOP elevation, we identified the *Grm4* mutation. Using IOP as a phenotype, we genetically mapped *Grm4* to a 1.7-Mb interval on chromosome 1 (**Fig. 4a**). We sequenced all of the genes in this region and identified a single nucleotide change in *1700027L20Rik*. Based on homology and functional data (see below), *1700027L20Rik* is now named *Prss56* (protease, serine, 56). From here on, we use $Prss56^{Grm4}$ to refer to homozygous mutant mice. The mutation in *Prss56* is a T to A transversion in exon 11 and disrupts a splice donor site (**Supplementary Fig. 2**). Intron 11 is retained in the mutant transcript, resulting in a small insertion followed by a premature stop codon (**Fig. 4b,c**). Notably, expression of the mRNA was substantially higher in mutant than in control eyes.

Based on the sequence homology of full length complementary DNA (cDNA), the protein encoded by *Prss56* appeared to be a secreted trypsin-like serine protease[14], with the catalytic domain being unaffected by the *Grm4* mutation (**Fig. 4d** and **Supplementary Fig. 3**). We tested if the protein has trypsin-like serine protease activity and determined that both the wild-type and mutant protein have this enzymatic activity (**Fig. 5a**). As expected for a secreted protein, wild-type and mutant proteins were localized in the endoplasmic reticulum (**Fig. 5b**). Our experiments using HEK293 cells suggest that both wild-type and mutant proteins are secreted, but with robust intracellular retention (**Fig. 5c**). Cellular fractionation experiments indicated that following signal peptide cleavage, Prss56 is no longer an integral membrane protein (**Fig. 5c**). However, the majority of cleaved wild-type and mutant protein is still membrane associated (as a peripheral membrane protein). Based on these data, Prss56 may function as both an extracellular and intracellular protease. Overall, our studies suggest that both the wild-type and mutant proteins behave similarly with respect to their subcellular localization and protease activity. Because the *Grm4* mutation does not affect protease activity with a synthetic substrate, the C terminus of Prss56 may have a critical regulatory function. The mutant C terminus may alter recognition of and/or specificity for endogenous substrate(s).

Prss56 is expressed in the retina (**Fig. 5d**). The retina is important for the postnatal determination of axial dimensions in response to visual experience in infants, a process that optimizes image focus on the retina (emmetropization)[15]. The molecular mechanism(s) linking the retina to axial elongation and refractive refinement are not understood. Because *Prss56* is expressed in the retina and acts in the postnatal determination of axial length (**Fig. 2f**), it is an excellent candidate to participate in emmetropization.

As shown above, mutation of *Prss56* affects ocular dimensions and results in high IOP, angle closure and choroidal expansion. The degree to which ocular dimensions are affected ranges from very little to severe depending on the genetic background (**Fig. 2** and **Supplementary Fig. 4**). In severe cases, there is a large reduction of axial length primarily caused by a decrease in posterior segment size (posterior microphthalmia). Proteases can directly or indirectly affect extracellular matrix (ECM) processing and degradation[16]. ECM changes caused by mutation of *Prss56* could affect all of these phenotypes.

The beams of the trabecular meshwork of mutant mice sometimes have very sparse ECM, and mutant sclerae have regions with abnormally packaged collagen fibrils (**Fig. 5e,f**), findings that are consistent with disturbed ECM as a pathological mechanism of the *Prss56* mutation. It is likely that ECM abnormalities contribute to altered ocular size and IOP elevation in ACG through a number of mechanisms. First, control of ECM synthesis and metabolism is important in ocular development[17]. Smaller eyes with relatively large lenses are predisposed to angle closure. Second, ECM abnormalities in the ocular drainage tissues are generally suggested to affect IOP in different forms of glaucoma[18–20] and may contribute to IOP elevation with increasing age in ACG. Multiple mechanisms of IOP elevation exist in at least a subset of individuals with ACG (combined mechanisms; see refs. 3,13). Third, altered iris ECM is speculated to contribute to IOP elevation and angle closure both by affecting iris permeability and by lessening the normal decrease of iris volume during dilation[7]. Fourth, altered scleral structure/composition and water/solute permeability are suggested to underlie choroidal effusion and expansion in ACG[10,21]. Choroidal effusion and expansion may push the lens and iris forward, thereby contributing to angle closure and IOP elevation[7].

Considering the range of ocular phenotypes in *Prss56*^{Grm4} mutant mice, we hypothesized that mutations in the human ortholog of *Prss56* may underlie various human phenotypes, including ACG and conditions with altered ocular size. Therefore, we analyzed the orthologous human gene in six human families with autosomal recessive posterior microphthalmia. Individuals with posterior microphthalmia have a reduced size of the ocular posterior segment and high hyperopia. These individuals usually have an ocular axial length of <20 mm. We selected these families because an independent effort showed that the gene underlying their phenotype was linked to a 2.3-Mb region containing *PRSS56* on 2q37.1 (ref. 22). Importantly and possibly relevant to glaucoma, at the last clinical evaluation, four individuals from families PM2 and PM3 had elevated IOP, with levels ranging from 26–30 mmHg. Moreover, two other individuals from family PM1 had optic nerve excavation.

Further linkage analysis refined the human interval to a 0.93-Mb critical region that included *PRSS56* (also named *LOC646960*; **Fig. 6a**). Importantly, we identified two mutations in this gene that specifically segregated with disease in families with microphthalmia (**Fig. 6b–d**). We identified no pathologic mutations in 17 other positional candidate genes that we assessed. A homozygous frameshift mutation (c.1059_1066insC, p.Gln356Pro*fs*X152; **Supplementary Fig. 5**) introduces a premature stop codon, leading to an altered protein with a 96-amino-acid C-terminal truncation (**Supplementary Fig. 6**). This mutation appears to be a founder mutation present in four families sharing the same pathologic haplotype[22]. The second mutation (a proline to alanine substitution, c.1795C>G, p.Pro599Ala) occurred

in one family (**Fig. 6d** and **Supplementary Fig. 5**). Like the *Grm4* mutation, both human mutations affect the C-terminal region of PRSS56. These data suggest that mutations in this gene may cause a spectrum of ocular defects in mice and humans. Only some mice, but all affected humans, had severe reductions in axial length caused by microphthalmia. Because the severe microphthalmia phenotype depended upon mouse genetic background, it is possible that the relatively homogenous genetic background in these consanguineous families contributed to lower phenotypic variation among these individuals (all with microphthalmia). Alternatively, both allelic variation and potential species differences could be important factors influencing phenotype. The presence of elevated IOP in some affected humans, as well as the presence of intrafamilial axial length variations, supports further evaluation of this gene in a spectrum of human conditions including ACG.

In summary, this study characterizes a new gene for ACG in mice and provides a much needed animal model for future research. It also links a new serine protease to the postnatal determination of axial length, a process that is critical for refinement of vision in all infants[15,23]. Future efforts to better characterize *PRSS56* and the potential contribution of genetic variants in this gene to a spectrum of ocular phenotypes, including changes in the size of the eye, hyperopia and ACG in affected individuals, are needed. Experiments are underway to evaluate its role in various conditions, with high priority on acute ACG, which often presents as a medical emergency.

ONLINE METHODS

Animal husbandry

All animals were treated in accordance with the protocols established by the Association for Research in Vision and Ophthalmology. The Animal Care and Use Committee of The Jackson Laboratory (Bar Harbor, Maine, United States) approved all experimental animal protocols.

Human subjects

We investigated six Tunisian families affected with isolated posterior microphthalmia. Informed consent was obtained from all participants and the parents of subjects younger than 18 years old (**Supplementary Note**). Detailed clinical evaluation was reported previously[22]. In brief, clinical exploration identified high hyperopia, elevated papillomacular retinal fold and a foreshortening of axial length with normal corneal diameter in all affected individuals. In some of these individuals, various posterior segment complications (for example, choroidal folds, uveal effusion syndrome and crowded optic disks) were observed[22].

N-ethyl-*N*-nitrosourea (ENU) mutagenesis

C57BL/6J (B6) males were mutagenized with ENU administered in three weekly injections of 80 mg/kg. A phenotype-driven recessive screen was performed to detect mutant mice with high IOP.

Intraocular pressure and outflow measurement

IOP was measured as previously described[24]. During the screen for mutants, high IOP was defined as IOP ≥ 3 s.d. above the population mean for the genetic context that we used (>19 mm of Hg). A family was designated as having high IOP if two or more progeny (out of 12 to 24) had an IOP > 19 mm Hg. The progeny were screened multiple times between 3 and 18 months of age. Outflow facility (C_t) was determined as described previously[25]. Outflow was recorded from six sex- and age-matched mice of each genotype.

Clinical slit-lamp analysis

Eyes were examined as previously reported[26]. Phenotypic evaluation included considerations for iris structure, pupillary abnormalities, cataract and the overall dimensions of the anterior chamber. Although we assessed IOP measurements at multiple ages, IOP is a dynamic phenotype and may not be high at a specific time of assessment. Although there was not a perfect relationship, there was a strong correlation between eyes that have had high IOP and enlarged anterior chamber. Thus, the presence of an enlarged anterior chamber was considered an important phenotype in our mapping strategy.

Ocular histological analysis and electron microscopy

Eyes were processed and analyzed as previously described[27] at ages ranging from postnatal day 7 and 20 months. More than 30 mutant and wild-type eyes were analyzed by a masked investigator.

Optic nerve analysis

Optic nerves were processed and analyzed as previously described[28]. Multiple masked investigators determined the degree of nerve damage, classifying nerves as: no, no glaucomatous axonal damage or unaffected; moderate, between 10% and 50% of the axons being damaged or lost; or severe, >50% axonal damage and/or loss. Each age group contained samples from males and females, as well as left and right optic nerves.

Measurement of ocular dimensions and choroidal thickness

Ocular axial length (anterior to posterior), equatorial diameter (nasal to temporal) and lens diameter were measured using a Vernier caliper following ocular enucleation (Fowler Ultra-Cal Mark III). At least six eyes were analyzed in each group. Axial length measurements for adult mice were performed at 2 months, at which age *Grm4* mutant mice did not have enlarged anterior chambers. Slit-lamp examination was performed before enucleation to ensure that measured eyes had a normal anterior chamber depth. In addition, we used a magnifying glass to ensure that the calipers were positioned accurately. Lenses were dissected and carefully checked for any attached tissue or debris.

For anterior and posterior segment measurements, enucleated wild-type and mutant eyes were positioned along the anterior-posterior axis. Images were taken using a dissection microscope fitted with a camera. Posterior segment length was measured as the maximum distance from the equator to the sclera in a straight line along the anterior to posterior axis of the eye. Anterior segment length was measured as the maximum distance from the equator

to the cornea. The line segment function in Fiji (image processing package based on ImageJ) was calibrated to provide values in millimeters.

Ocular histological sections were used to measure choroidal thickness. All the images were acquired at 20× magnification. We measured choroidal thickness in three locations spaced approximately 300 μm apart and located halfway between the optic nerve head and iris root. The line segment function in Fiji was calibrated to provide values in micrometers, and the average value for each eye was used.

Evaluation of the angle *in vivo*

For gonioscopy, the iridocorneal angle was clinically monitored with a goniolens as described previously[29]. Optical coherence tomography (OCT; Bioptigen, Inc) was used to assess the *in vivo* angle configuration. Mice were anesthetized and their eyes were hydrated using lubricant eye gel (GenTeal Severe Gel, Novartis). Mice were secured on a freely rotating stage. To view the deep angle region that contains the drainage structure, the eyes were slightly proptosed by very gentle use of a Q-tip. The Q-tip was removed and the eyes remained in this position for imaging. Volumetric images of the angle located in the temporal quadrant were acquired for each mouse. Mice were first aligned so that the OCT laser path ran along the optical axis of the eye. The Purkinje reflection was obtained on both X and Y images to confirm that the laser was normal to the apex of the cornea. The mice were then swiveled laterally (while maintaining other planes) so that the laser beam passed through the corneoscleral junction and reached the angle. Images were acquired from six mutant and six wild-type mice. Averaged linear scans are presented.

Provocative tests for angle closure

Pupillary dilation with cyclopentolate acts as a provocative test for IOP elevation induced by angle closure in humans[3,13]. Mutant and wild-type mice (11 weeks old) were subject to pupillary dilation with a drop of 1% solution of cyclopentolate that was topically applied to the cornea (Bausch and Lomb). At this age, none of the mice had high IOP without provocation. Two hours after dilation, the mice were injected intraperitoneally with water (0.5 ml per 10 g bodyweight) to increase the aqueous inflow. Mice were anesthetized 15 min after water injection, and their IOP was immediately measured. In a parallel experiment, 2 h after dilation, wild-type and mutant eyes were examined with a slit lamp to assess their anterior chamber depth.

Mapping *Grm4*

To map the *Grm4* mutation, mutant B6 mice were crossed to a C3H/HeJ derived strain C3A.BLiA-*Pde6b*$^{+}$/*J* (C3A.BLiA, stock # 001912). All F1 mice were phenotypically normal. We used a backcross strategy to map the gene. A total of more than 1,000 N2 progeny were aged, and their IOP was measured between 1 and 9 months of age. Initial genotyping was performed using over 100 genome-wide SNPs (KBioscience, UK). Fine mapping of the critical interval was performed using established and newly synthesized markers. After progeny testing of N2 mice with critical recombination events, the minimal genetic region of *Grm4* was identified as a 1.7-Mb interval on chromosome 1.

Sequencing of *1700027L20Rik*

Genomic DNA from homozygous mutant mice (n = 7) and from C57BL/6J mice (n = 5) was amplified using the primers (**Supplementary Table 1**). RNA was extracted, and cDNA was sequenced for five homozygous mutant eyes and five control eyes.

Genotyping and genetic background

Mice were genotyped with an allele-specific PCR protocol to distinguish wild-type from mutant mice using primer pairs presented in **Supplementary Table 1**. For **Figure 1** and **Supplementary Figure 1**, the data are for mice with a largely B6 genetic background (average >75% as B6 × C3A. BLiA progeny were backcrossed to B6 for one (N2) or two generations (N3)). Everywhere else, other than in **Supplementary Figure 4**, the mice were also largely B6 (>99%, generation ≥N6 with the majority ≥N8). For **Supplementary Figure 4**, the mice had a largely C3A.BLiA genetic background (>99%, *Grm4* mutation backcrossed to C3A.BLiA for ten generations (N10)).

Cloning of full length *Prss56* and generation of expression constructs

Full length wild-type *Prss56* (*Prss56*^{WT}) and *Prss56*^{Grm4} cDNA was amplified with primers given in **Supplemenetary Table 1**. PCR products were digested with EcoRI and XhoI (New England Biolabs) and subcloned into PCMV-3Tag-3a (Agilent Technologies) to facilitate generation of C-terminal FLAG-tag fusion protein. Because the N terminus signal peptide is cleaved subsequent to its endoplasmic reticulum targeting, we ensured that the FLAG-tag was inserted in the C terminus of the protein. We also generated an N-terminal FLAG-tag fusion protein by subcloning the insert into PCMV-3Tag-1A (Agilent Technologies) to confirm that the N terminus sequence functioned as a signal peptide.

Serine protease activity

Culture supernatants from HEK293 cells expressing recombinant wild-type and mutant protease were concentrated using Amicon Ultra-15 Filter Units (Cat # UFC801008, Milipore) and used as sources to assess protease activity. Supernatants from mock transfected HEK293 cells were used as a control. The amount of wild-type and mutant protein was comparable, as assessed by protein blot analysis. We performed three independent experiments, each in triplicate. Fluoregenic assays were performed in a 96-well plate by measuring the release of free aminomethylcoumarin (AMC) from the substrate Z-Gly-Gly-Arg-AMC (Bachem). The protease activity was assessed in buffer containing 50 mM Tris–HCl (pH 8.0), 10 mM $CaCl_2$, 100 mM NaCl and 1 μM Z-Gly-Gly-Arg-AMC in presence or absence of 1 μM TLCK (inhibitor of trypsin-like serine protease). Fluorescence intensity was measured with a spectrofluorimeter plate reader (Molecular Devices) set at 390 nm (excitation wavelength) and 460 nm (emission wavelength).

Subcellular fractionation

To assess the subcellular localization of the Prss56 protein, we performed fractionation studies. HEK293 cells were split into six-well plates and grown to 80% confluency. Each well was transfected with 1 μg plasmid DNA using Lipofectamine 2000 (Invitrogen). Cells were harvested 12–18 h after transfection. Transfected HEK293 cells were homogenized in

normal lysis buffer (20 mM Tris (pH 7.4), 150 mM NaCl, with protease inhibitor cocktail (Roche cat # 04693124001)) or alkaline lysis buffer (20 mM Tris (pH 7.4), 700 mM NaCl, 1 mM $MgCl_2$ and 1 mM $CaCl_2$ with 50 mM NaOH with protease inhibitor cocktail). The cell suspension was homogenized by passing it through a 30-gauge needle four times, and the homogenate was centrifuged at 100,000 *g* for 30 min. The supernatant was centrifuged again at 100,000 *g* for 30 min, and the resulting supernatant used as the soluble fraction. Membrane pellets were solubilized in lysis buffer with 1% Triton X-100, centrifuged at 16,000 *g* for 20 min and used as the membrane fraction. All steps were carried out on ice. The fractions were resolved on SDS-PAGE and protein blotted. Immunodetection was performed using Mouse Anti-FLAG M2 Monoclonal Antibody (Sigma-Aldrich, 1: 1000 dilution). Calnexin, an endoplasmic reticulum localized transmembrane protein, was used as a marker to rule out membrane contamination in the soluble fractions using a Calnexin antibody (Enzo Life Sciences; 1:1000 dilution). All experiments were independently conducted at least three times.

Quantitative PCR (qPCR)

qPCR examined the relative expression levels of *Prss56* mRNA in individual eyes in both wild-type ($n = 5$) and mutant ($n = 5$) mice between 1 and 3 months of age. Primer pairs used for qPCR of an 83-bp region spanning exon 4 and exon 5 are given in **Supplementary Table 1**. To analyze the qPCR data, we used the statistical algorithm global pattern recognition (GPR)[30].

In situ hybridization

In situ hybridization was performed on 20 μm fresh frozen retinal sections using Dig-labeled riboprobe and standard procedures. The gene-specific probes used were designed using the primers listed in **Supplementary Table 1**. The hybridized mRNA was detected using the Tyramide Signal Amplification System (Perkin-Elmer).

Genetic linkage in families with posterior microphthalmia

To refine the human chromosome 2 critical interval, all participating family members were genotyped using informative fluorescent dye-labeled microsatellite markers referenced to the UCSC Human Genome database (see URLs). We also generated, within the 2q37.1 region, four new microsatellite markers: D2S16AC, D2S22AC, D2S25AC and D2S24AC. The PCR primers for these markers are given in **Supplementary Table 1**. These analyses were performed on an ABI PRISM 3100-Avant automated DNA sequencer (Applied Biosystems, USA). Genotypes were determined using the GenScan and GenoTyper software (Applied Biosystems).

Mutation analysis of *PRSS56*

All exons and intron-exon boundaries of 17 candidate known genes in the refined 2q37.1 interval were amplified under standard PCR conditions. Sequences of primers used for the amplification of the uncharacterized orthologous *PRSS56* gene are given in **Supplementary Table 1**. All PCR products of one affected subject from each family were sequenced using the amplification primers on an ABI 3100-Avant automated DNA sequencer and the Big

Dye Terminator Sequencing Kit (Applied Biosystems) according to the manufacturer's instructions. To verify mutations, the appropriate *PRSS56* exons were then amplified by PCR and sequenced in all available family members. Screening for the c.1795C>G mutation in the control population was carried out by PCR-restriction fragment length polymorphism (PCR-RFLP) analysis using the Tau1 restriction enzyme.

Statistical analyses

Statistical comparisons were performed using a Student's two-tailed unpaired *t* test except when comparing optic nerve distribution, for which a χ^2 analysis was used.

Supplementary Material

Refer to Web version on PubMed Central for supplementary material.

ACKNOWLEDGEMENTS

The authors thank A. Bell, S. Kneeland, H. McLaughlin, A. Gillette, M. Ryan, Annette Molbaek, Åsa Schipper and The Jackson Laboratory's Fine Mapping Service and Allele Typing and Sequencing services for technical assistance. We thank P. Nishina for generous use of her OCT and J. Vance of Bioptigen for his expert technical assistance, G. Cox, P. Nishina and M. de Vries for comments on the manuscript and J. Hammer for help with graphics. The National Eye Institute Grant EY11721, Barbara and Joseph Cohen Foundation, Ministère de l'Enseignement Supérieur, de la Recherche Scientifique et de la Technologie >> Tunisia, the Middle East and North Africa region (MENA) [Swedish research links programme supported by the Swedish Research Council(VR)/the Swedish International Development Cooperation Agency (SIDA) and the Project 2006 planning grant # 348-2005-6336 supported this work. S.W.M.J. is an Investigator of the Howard Hughes Medical Institute. We thank the family members for their valuable participation and cooperation.

References

1. Quigley HA. Number of people with glaucoma worldwide. Br. J. Ophthalmol. 1996; 80:389–393. [PubMed: 8695555]
2. Ritch, R.; Lowe, RF. Angle-closure glaucoma: mechanisms and epidemioilogy.. In: Ritch, R.; Shields, MB.; Krupin, T., editors. The Glaucomas. Mosby-Year Book, Inc.; St. Louis, Missouri: 1996. p. 801-819.
3. Shields, MB. Pupillary-block glaucomas.. In: Cooke, DB., editor. Textbook of Glaucoma. Williams & Wilkens; Baltimore, Maryland, USA: 1996. p. 177-194.
4. Seah SK, et al. Incidence of acute primary angle-closure glaucoma in Singapore. An island-wide survey. Arch. Ophthalmol. 1997; 115:1436–1440. [PubMed: 9366676]
5. Foster PJ, Johnson GJ. Glaucoma in China: how big is the problem? Br. J. Ophthalmol. 2001; 85:1277–1282. [PubMed: 11673287]
6. Lowe RF. Aetiology of the anatomical basis for primary angle-closure glaucoma. Biometrical comparisons between normal eyes and eyes with primary angle-closure glaucoma. Br. J. Ophthalmol. 1970; 54:161–169. [PubMed: 5428641]
7. Quigley HA. Angle-closure glaucoma-simpler answers to complex mechanisms: LXVI Edward Jackson Memorial Lecture. Am. J. Ophthalmol. 2009; 148:657–669. [PubMed: 19878757]
8. Sakai H, et al. Uveal effusion in primary angle-closure glaucoma. Ophthalmology. 2005; 112:413–419. [PubMed: 15745767]
9. Hrabé de Angelis MH, et al. Genome-wide, large-scale production of mutant mice by ENU mutagenesis. Nat. Genet. 2000; 25:444–447. [PubMed: 10932192]
10. Elagouz M, Stanescu-Segall D, Jackson TL. Uveal effusion syndrome. Surv. Ophthalmol. 2010; 55:134–145. [PubMed: 20159229]

11. Kumar RS, et al. Confirmation of the presence of uveal effusion in Asian eyes with primary angle closure glaucoma: an ultrasound biomicroscopy study. Arch. Ophthalmol. 2008; 126:1647–1651. [PubMed: 19064843]
12. Quigley HA. What's the choroid got to do with angle closure? Arch. Ophthalmol. 2009; 127:693–694. [PubMed: 19433722]
13. Ritch, R. Angle-closure glaucoma: clinical types.. In: Ritch, R.; Shields, MB.; Krupin, T., editors. The Glaucomas, Clinical Science. Vol. 2. Mosby Year Book; St. Louis, Missouri: 1996. p. 821-840.
14. Ross J, Jiang H, Kanost MR, Wang Y. Serine proteases and their homologs in the Drosophila melanogaster genome: an initial analysis of sequence conservation and phylogenetic relationships. Gene. 2003; 304:117–131. [PubMed: 12568721]
15. Rymer J, Wildsoet CF. The role of the retinal pigment epithelium in eye growth regulation and myopia: a review. Vis. Neurosci. 2005; 22:251–261. [PubMed: 16079001]
16. Mott JD, Werb Z. Regulation of matrix biology by matrix metalloproteinases. Curr. Opin. Cell Biol. 2004; 16:558–564. [PubMed: 15363807]
17. Hausman RE. Ocular extracellular matrices in development. Prog. Retin. Eye Res. 2007; 26:162–188. [PubMed: 17185022]
18. Tektas OY, Lutjen-Drecoll E. Structural changes of the trabecular meshwork in different kinds of glaucoma. Exp. Eye Res. 2009; 88:769–775. [PubMed: 19114037]
19. Keller KE, Aga M, Bradley JM, Kelley MJ, Acott TS. Extracellular matrix turnover and outflow resistance. Exp. Eye Res. 2009; 88:676–682. [PubMed: 19087875]
20. Fleenor DL, et al. TGFβ2-induced changes in human trabecular meshwork: implications for intraocular pressure. Invest. Ophthalmol. Vis. Sci. 2006; 47:226–234. [PubMed: 16384967]
21. Jackson TL, et al. Scleral hydraulic conductivity and macromolecular diffusion in patients with uveal effusion syndrome. Invest. Ophthalmol. Vis. Sci. 2008; 49:5033–5040. [PubMed: 18552396]
22. Hmani-Aifa M, et al. A genome-wide linkage scan in Tunisian families identifies a novel locus for non-syndromic posterior microphthalmia to chromosome 2q37.1. Hum. Genet. 2009; 126:575–587. [PubMed: 19526372]
23. Mutti DO, et al. Axial growth and changes in lenticular and corneal power during emmetropization in infants. Invest. Ophthalmol. Vis. Sci. 2005; 46:3074–3080. [PubMed: 16123404]
24. John SWM, Hagaman JR, MacTaggart TE, Peng L, Smithes O. Intraocular pressure in inbred mouse strains. Invest. Ophthalmol. Vis. Sci. 1997; 38:249–253. [PubMed: 9008647]
25. Aihara M, Lindsey JD, Weinreb RN. Aqueous humor dynamics in mouse. Invest. Ophthalmol. Vis. Sci. 2003; 44:5168–5173. [PubMed: 14638713]
26. Anderson MG, et al. Mutations in genes encoding melanosomal proteins cause pigmentary glaucoma in DBA/2J mice. Nat. Genet. 2002; 30:81–85. [PubMed: 11743578]
27. Smith, RS.; Sundberg, JP.; John, SWM. The Anterior Segment. In: Smith, RS.; John, SWM.; Nishina, PM.; Sundberg, JP., editors. Systematic Evaluation of the Mouse Eye: Anatomy, Pathology and Biomethods. Vol. 366. CRC Press; Boca Raton, Florida, USA: 2002.
28. Howell GR, et al. Axons of retinal ganglion cells are insulted in the optic nerve early in DBA/2J glaucoma. J. Cell Biol. 2007; 179:1523–1537. [PubMed: 18158332]
29. Smith RS, Korb D, John SWM. A goniolens for clinical monitoring of the mouse iridocorneal angle and optic nerve. Mol. Vis. 2002; 8:26–31. [PubMed: 11889463]
30. Akilesh S, Shaffer DJ, Roopenian D. Customized molecular phenotyping by quantitative gene expression and pattern recognition analysis. Genome Res. 2003; 13:1719–1727. [PubMed: 12840047]

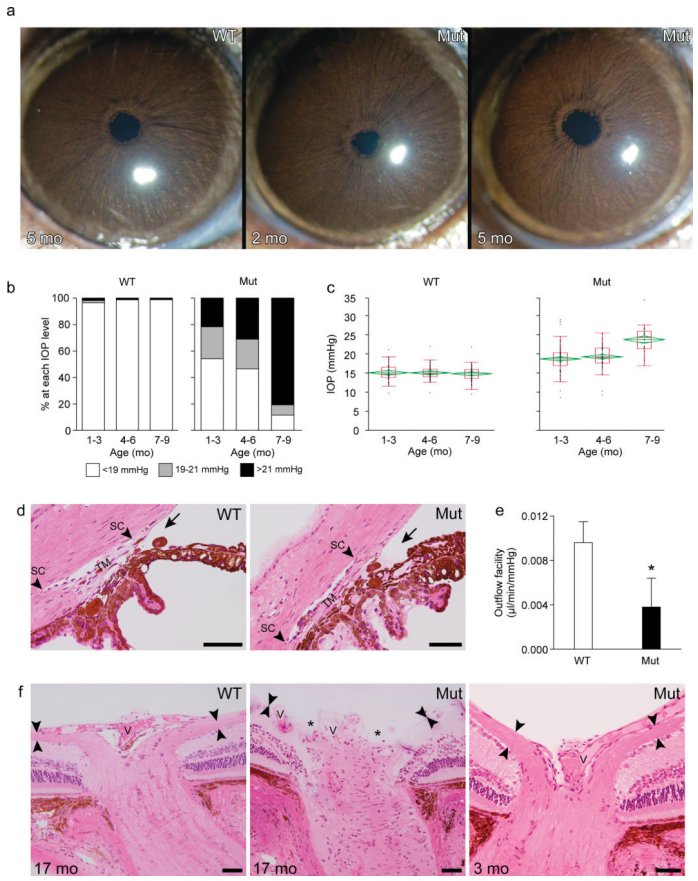

Figure 1.

Grm4 mutant mice have normal angle tissues and exhibit high IOP. (**a**) We subjected mice to slit-lamp examination by broad-beam illumination to assess ocular structures including the iris, pupil and lens. We compared mutant mice (Mut) to age-matched wild-type (WT) mice. Representative eyes of mice of the indicated ages are shown. We detected no obvious structural abnormalities in mutant eyes. (**b,c**) IOP distributions for wild-type and mutant mice. Mutant eyes had significantly higher IOP compared to wild-type at all ages (*t* test $P < 0.0001$). In the box plots (**c**), the green line and surrounding diamonds represent the mean ± s.e.m. (total $n \geq 170$ for each genotype, and total $n \geq 30$ for each group). (**d**) Histological analysis of angles showing well-formed trabecular meshwork (TM) and Schlemm's canal (SC, arrowheads) drainage tissues. There was no abnormal tissue obstructing the angle recess (arrow). (**e**) Mean outflow facility ± s.d. of wild-type and mutant eyes. Total outflow (Ct) is significantly reduced in mutant mice (*$P < 0.0001$, *t* test, $n = 6$ for each genotype). (**f**) Histological assessment of optic nerve heads. Mutant but not wild-type eyes exhibit hallmarks of glaucomatous nerve damage, including optic nerve excavation (asterisk) and thinning of the nerve fiber layer with age (arrow heads). V, blood vessels. Scale bar, 50 µm.

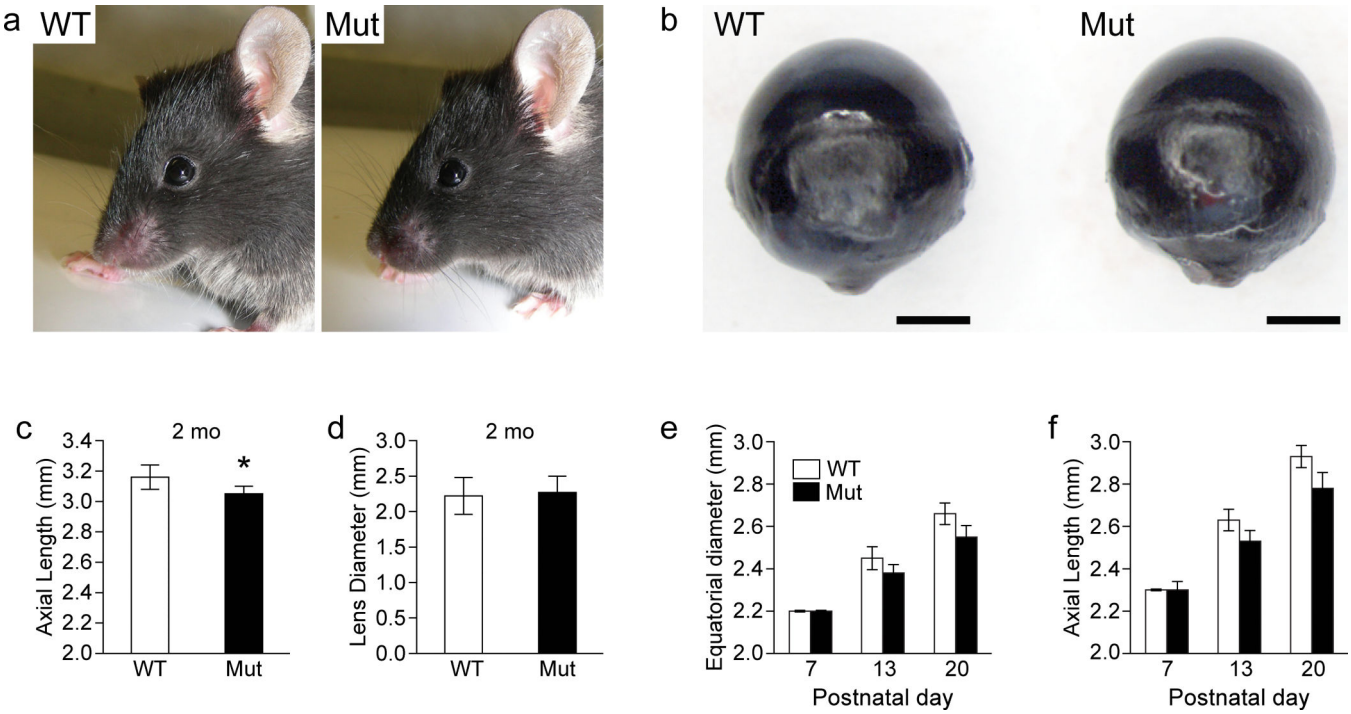

Figure 2.

Grm4 mutant eyes have short axial length. (**a**) Photographs showing no obvious difference in ocular size between wild-type and mutant mice. (**b**) Close evaluation of enucleated eyes indicates that mutant eyes with a largely B6 strain background (>99% B6; Online Methods) are slightly smaller than wild-type eyes. **c)** The mutant eyes are about 4.4% shorter than wild-type eyes (*$P = 0.015$, *t* test). (**d**) The lens diameter of the wild-type and mutant eyes was the same ($P = 0.27$, *t* test). (**e,f**) The differences in ocular size occured after postnatal day 7. The ocular axial length and equatorial diameter was significantly smaller at P13 and P20 ($P < 0.01$, *t* test). All histograms are mean ± s.d. and $n \geq 6$ for all groups. Scale bar in **b**, 1 mm.

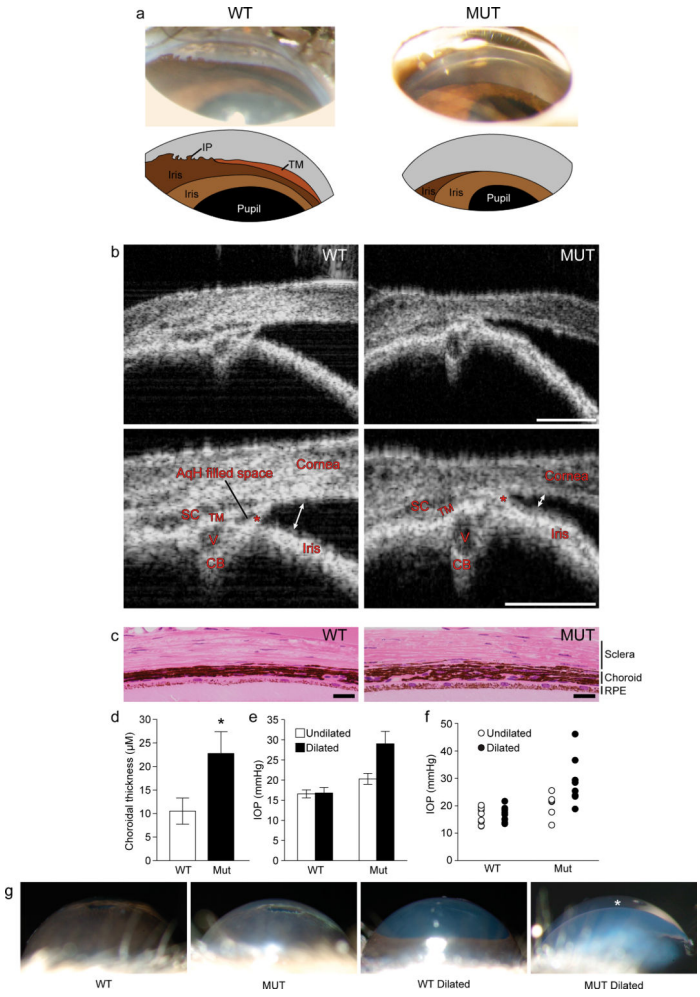

Figure 3.

Angle closure and choroidal expansion in *Grm4* mutant mice. (**a**) Goniophotographs of wild-type and mutant angles with corresponding schematic diagrams. The darker iris shade represents regions that were less illuminated. Key angle structures, the iris process (IP) and lightly pigmented trabecular meshwork (TM), are clearly visible in wild-type eyes. Because the iris prevents viewing of the angle, these structures were not visible in any mutant eyes. (**b**) OCT images of the temporal angle. The bottom panels are enlarged views of the same images to label ocular structures: ciliary body (CB), iris vessel (V), Schlemm's canal (SC), trabecular meshwork (TM) and iris strand (asterisk). When using OCT, fluid-filled spaces appear dark. AqH has unobstructed access to the drainage structures in wild-type eyes. This appears as a dark AqH-filled region that is deeper in the angle than in the iris strand. This space is absent in mutants, as the iris strand and iris are closely apposed to the trabecular meshwork. Additionally, the deep angle recess is much narrower in mutant eyes (double headed arrows). (**c**) Histologically, the mutant choroid is expanded and thicker than the wild-type choroid at 2 months of age. (**d**) Choroidal thickness (mean ± s.d., $*P < 0.001$, *t* test, $n = 5$ for each genotype). (**e**) Mean IOP ± s.e.m. with and without pupil dilation and (**f**) a scatter plot of the same data. Following dilation, the IOP of some mutant eyes increased substantially (up to 46 mm Hg). (**g**) Consistent with increased IOP, pupil dilation caused a

substantial anterior chamber enlargement in mutant (asterisk) but not wild-type eyes. Scale bars in **b**, 100 μm; scale bars in **c**, 20 μm.

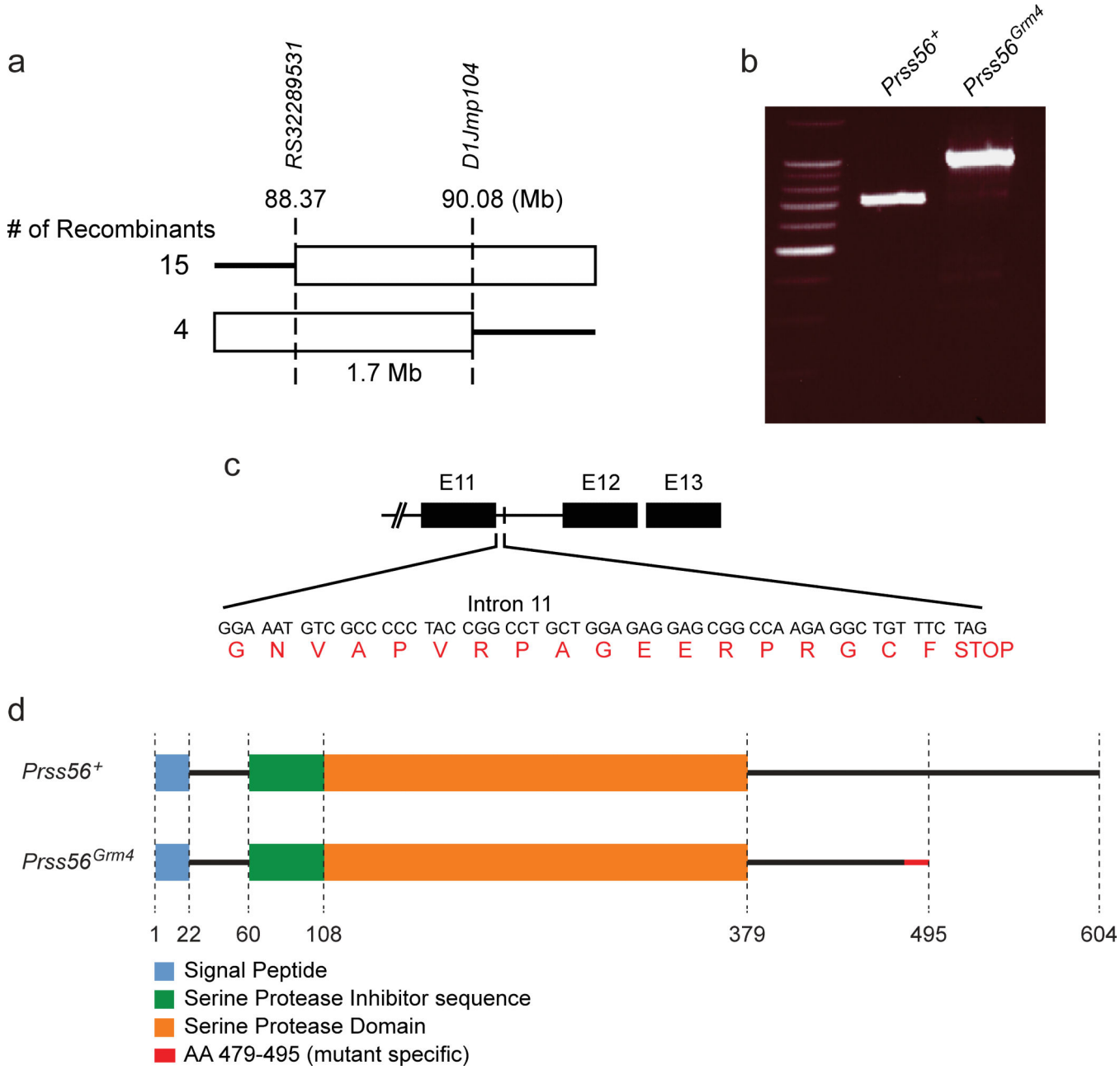

Figure 4.

Grm4 is a serine protease mutation. (**a**) Map of the critical interval defined using approximately 1,000 backcross mice. The thin lines indicate the chromosomal regions excluded by recombination, with numbers of independent recombinants defining the critical interval indicated on the left. Genetic mapping localized the *Grm4* mutation to a 1.7-Mb region on chromosome 1 flanked by the SNP marker rs32289531 (88,377,699; National Center for Biotechnology Information (NCBI) mouse Build 37) and the SSLP marker D1Jmp104 (90,084,181–90,084,437; Ensembl Build 37). (**b**) RT-PCR of *Prss56* cDNA, using primers that amplify regions of exon 11 through exon 13, gives a product of 695 bp in the wild type and 980 bp in mutant as a consequence of intron 11 retention. (**c**) Translation

of the intronic region results in addition of 17 amino acids after glycine, which are not present in wild-type protein and are followed by a stop codon. (**d**) Schematic representation of wild-type and mutant forms of the Prss56 protease. The protein contains a signature N-terminal signal peptide (blue box), a serine protease inhibitor domain (green box) and a serine protease domain (orange box). Translation of intron 11 results in 17 amino acids that are specific to the mutant (red line). The mutant protein is truncated and lacks the normal terminal 109 amino acids.

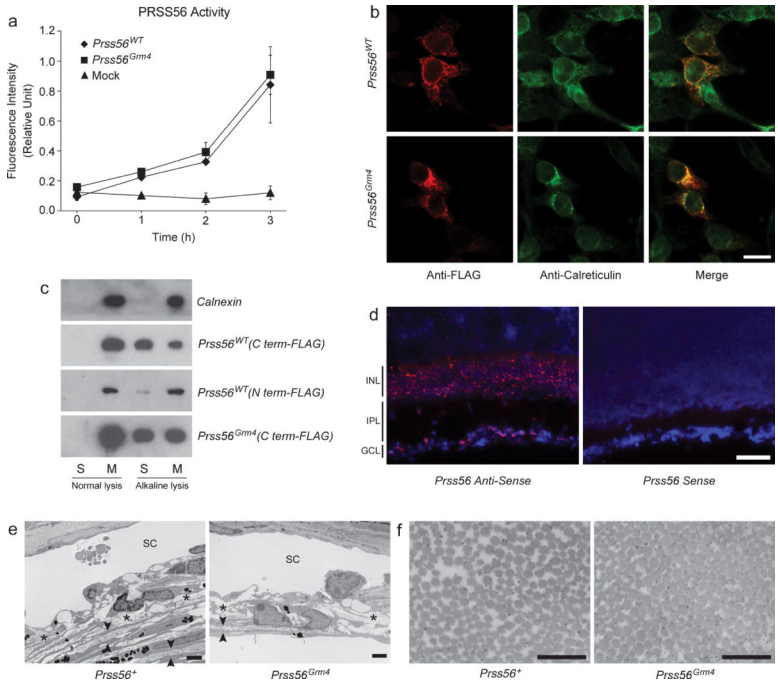

Figure 5.

Characterization of the Prss56 protease. (**a**) Both wild-type and mutant protein show trypsin-like serine protease activity (mean ± s.d. of three independent experiments). (**b**) HEK293 cells expressing wild-type or mutant Prss56 were analyzed by immunofluorescence microscopy. Both the mutant and wild-type protease co-localize with calreticulin, supporting endoplasmic reticulum localization. (**c**) Protein blot analysis of membrane (M) and soluble (S) fractions from HEK293 cells overexpressing C- and N-terminal FLAG-tagged protein. Both wild-type and mutant C terminus FLAG- tagged Prss56 proteins are detected in the soluble fraction after alkaline lysis, suggesting that they are not integral membrane proteins. However, the majority of N terminus FLAG-tagged Prss56 is detected in the membrane fraction after alkaline lysis, suggesting that signal peptide cleavage is required for membrane release. Calnexin is a marker of integral membrane proteins. (**d**) *In situ* hybridization shows that *Prss56* mRNA is expressed in the retina, mainly in the inner nuclear layer (INL) and ganglion cell layer (GCL). (**e**) Electron micrographs (EM) showing that trabecular meshwork (TM) of mutant but not wild-type mice are focally hypoplastic, with substantially reduced collagen fibrils in the trabecular beams (between the two arrowheads) and have more open spaces lacking ECM (asterisks). (**f**) An electron micrograph shows that mutant sclera has focal regions with abnormal crowding of collagen fibrils, suggesting altered ECM assembly in the sclera. We did not observe such crowded regions in wild-type eyes. Scale bars in **b**, 20 μm; scale bars in **d**, 50 μm; scale bars in **e**, 2 μm; scale bars in **f**, 0.5 μm.

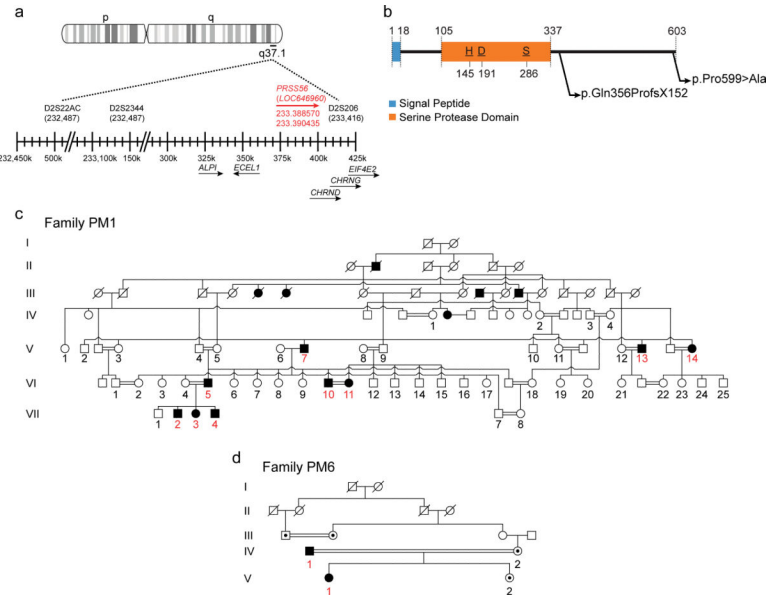

Figure 6.

Linkage interval and mutation analysis of *PRSS56* in Tunisian families with posterior microphthalmia. (**a**) Human chromosome 2 region showing the refined critical linkage interval (0.93 Mb) flanked by microsatellite markers D2S22AC and D2S206. The positions of *PRSS56* (*LOC646960*) and some neighboring genes are indicated. (**b**) The positions of mutations identified in the PRSS56 protein are shown. An important catalytic triad of conserved amino acids in the serine protease domain is shown (H, histidine; D, aspartate; S, serine). (**c**) In family PM1, all individuals homozygous for the insertion (c.1059_1066insC) showed high hyperopia (numbered in red). No unaffected family members were homozygous for the mutation. The mutation also segregated with posterior microphthalmia in four other families but was not present in 60 population matched controls. (**d**) In family PM6, homozygosity for a missense mutation (c.1795C>G) segregated with microphthalmia. This mutation was not present in 88 population matched controls.